Communication

Optimization of Microwave Wireless Power Transmission With Specific Absorption Rate Constraint for Human Safety

Ho Yeol Kim and Sangwook Nam

***Abstract*— In this communication, we propose a new convex optimization algorithm for exciting the transmitting antennas of a microwave wireless power transmission (MPT) system that transfers maximum power under a specific absorption rate (SAR) constraint for human safety. The transformation of the initial NP-hard problem to a convex optimization problem is described in detail. We applied the proposed algorithm to several MPT scenarios with multiple transmitting antennas around and one receiver placed near a box-shaped phantom model. The channel response and the electric field response for the receiver and phantom required for the optimization process are obtained using full-wave electromagnetic simulations. The received power and the power transfer efficiency (PTE) of the proposed optimization (OPT) technique are compared with those of the time-reversal (TR) technique at 0.9 GHz. The results show that the OPT technique can transfer more power than the TR technique with a lower PTE within the SAR limit and that the proposed technique can be applied to various MPT scenarios.**

***Index Terms*— Convex optimization, human safety, maximum received power, microwave wireless power transmission (MPT), specific absorption rate (SAR), time reversal (TR).**

I. Introduction

Microwave wireless power transmission (MPT) has been an area of research since the 1960s and is nowadays attracting increasing attention owing to the widespread use of wireless devices, such as mobile phones, Internet-of-Things devices, sensors, and implant devices [1], [2]. Various types of MPT have been studied theoretically and experimentally [1]–[13]. Large phased array for long-distance MPT was studied in the 1960s [3], [4], and MPT techniques using retro-directive arrays [5], [6] and time-reversal (TR) techniques for indoor environments [7]–[10] have also been reported. In addition, waveform design for improving the RF–dc efficiency of a rectifier has been investigated [11], [12].

The goal in the MPT research is to transfer the maximum power from a transmitter to a receiver. TR technique is known as the optimum technique for maximizing wireless power transfer efficiency (PTE) in free space [7]; it flips the received signal in time to refocus the original field as an incoming wave [8] and can be interpreted as a phase-conjugation technique in the frequency domain. In practical cases, the electromagnetic field (EMF) cannot be fully restored using a finite transmitting antenna array and, hence, there is a PTE boundary in terms of the transmitting area and transfer distance [9]. Although TR is the best solution for MPT even in practical cases with maximum PTE, EMF issues should be considered when designing MPT systems.

Manuscript received January 13, 2020; revised February 28, 2020; accepted March 10, 2020. Date of publication March 24, 2020; date of current version October 29, 2020. This work was supported by the National Research Foundation of Korea (NRF) grant funded by the Korea Government (MSIP) under Grant 2016R1E1A1A01943375. *(Corresponding author: Sangwook Nam.)*

The authors are with the School of Electric and Computer Engineering, Institute of New Media Communication, Seoul National University, Seoul 151-742, South Korea (e-mail: hykim@ael.snu.ac.kr; snam@snu.ac.kr).

Color versions of one or more of the figures in this communication are available online at http://ieeexplore.ieee.org.

Digital Object Identifier 10.1109/TAP.2020.2981674

In general, electromagnetic (EM) waves cause thermal heating in the body and may be hazardous to humans. Therefore, the specific absorption rate (SAR), which measures the EM energy absorbed per unit mass of tissue, is used to limit EM wave exposure. An SAR limit of 1.6 W/kg averaged over 1 g of local tissue proposed in the ANSI/IEEE C95.1 standard was recommended by the Federal Communications Commission (FCC) [13]. In particular, the use of an MPT system close to the body makes it more dangerous than other wireless devices because MPT systems employ high power in their transmitter. Therefore, considering human safety is one of the most important issues in MPT research. A few researchers have checked whether their wireless power transfer (WPT) systems satisfy the SAR limit after system implementation [14]–[16]. However, human safety must be considered during the design process of WPT systems.

In this communication, we propose a convex optimization algorithm that can control the electric field (E-field) in the body not to exceed the SAR limit and transfer maximum power to the receiver when the receiver is positioned near body. A similar optimization technique was used in hyperthermia research to focus the E-field without input power constraints [17]. In this communication, we formulate the optimization algorithm that maximizes the power received by the receiver and includes a total input power constraint. The proposed algorithm is applied to several MPT scenarios with multiple transmitting antennas and one receiver near a box-shaped phantom model. Full-wave numerical simulation is used to compare the performance, received power, and PTE of the proposed optimization (OPT) technique with those of the TR technique. The differences in the performance for different distances and the worst case scenario are analyzed in detail. With the proposed optimization algorithm, the MPT system transfers more power to the receiver in every scenario compared with the TR technique.

The rest of this communication is organized as follows. Section II describes the formulation of the optimization problem and its transformation to a new convex optimization problem. The simulation and the results of the performance comparison of the OPT and TR techniques are presented in Section III. The main conclusions from the study are summarized in Section IV.

II. Optimization Problem

A. Optimization Problem Formulation

The optimization problem is formulated for an MPT scenario with N transmitting antennas around a receiving antenna located near a human phantom model, as shown in Fig. 1. When a unit voltage is applied to each transmitting antenna, the E-field produced by each antenna at position r in the human phantom model is expressed as

$$\overline{\overline{E}}(r) = \begin{bmatrix} e_{x0}(r) & e_{x1}(r) & \cdots & e_{xN-1}(r) \\ e_{y0}(r) & e_{y1}(r) & \cdots & e_{yN-1}(r) \\ e_{z0}(r) & e_{z1}(r) & \cdots & e_{zN-1}(r) \end{bmatrix}^T \tag{1}$$

where $e_{xn}(r)$, $e_{yn}(r)$, and $e_{zn}(r)$ refer to the x, y, and z components of the E-field at r in the phantom excited by the nth

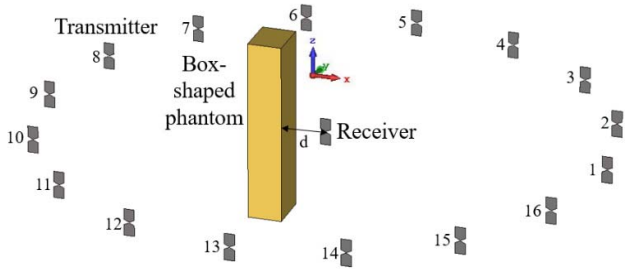

Fig. 1. 3-D MPT scenario with 16 transmitters and a receiver comprising bowtie half-lambda dipole antennas and a small box-shaped phantom near the receiver.

transmitting antenna, respectively. Consider a transmitting signal vector $\mathbf{S}=[s_0, s_1 \cdots s_{N-1}]^T$. The nth element of $\mathbf{S}$, $s_n = \upsilon_n e^{j\psi_n}$, represents the excitation of a complex voltage to the nth transmitting antenna, where υ_n and ψ_n are the amplitude and phase of the signal, respectively. The total E-field vector at position r in the human phantom model when the signal $\mathbf{S}$ is excited by N transmitting antennas is expressed as

$$\mathbf{E}(r,\mathbf{S}) = \overline{\overline{E}}(r)^T\mathbf{S} = \begin{bmatrix} E_x(r,\mathbf{S}) \\ E_y(r,\mathbf{S}) \\ E_z(r,\mathbf{S}) \end{bmatrix} \tag{2}$$

where $E_x(r,\mathbf{S})$, $E_y(r,\mathbf{S})$, and $E_z(r,\mathbf{S})$ are the x, y, and z components of the E-field, respectively. The components of the E-field vector are expressed as $\sum_{n=0}^{N-1} e_{xn}(r)s_{xn}$, $\sum_{n=0}^{N-1} e_{yn}(r)s_{yn}$, and $\sum_{n=0}^{N-1} e_{zn}(r)s_{zn}$, respectively. In the proposed optimization problem, (2) is used to formulate the SAR constraint. The received voltage on the receiving antenna can be obtained as $V_R(\mathbf{S}) = \sum_{n=0}^{N-1} h_n s_n = \mathbf{H}^T\mathbf{S}$ with $\mathbf{H}=[h_0, h_1 \cdots h_{N-1}]^T$, where $h_n = A_n e^{j\phi_n}$ is the channel response between the nth transmitting antenna and the receiver. A_n and ϕ_n are the amplitude and phase of the channel response, respectively.

With the channel response and the E-field, the optimal transmitted signal $\mathbf{S}$ should be found to maximize the received power considering the limit of the total transmitted power and the SAR constraint, that is

$$\max \ P_R(\mathbf{S}) \tag{3}$$

$$\text{s.t.} \ \frac{\|\mathbf{S}\|_F^2}{R} \le P \tag{4}$$

$$\frac{\sigma\,|\mathbf{E}(r,\mathbf{S})|_F^2}{\rho} \le SAR, \quad r \in \Psi. \tag{5}$$

$P_R(\mathbf{S})$ is the target function and is proportional to the received power at the receiver. $P_R(\mathbf{S})$ can be expressed as $|V_R(\mathbf{S})|^2$. The limited transmitted power constraint is expressed in (4), where R and P refer to the radiation resistance of the transmitting antenna under matching conditions and the total transmitted power, respectively. The SAR regulation in the human phantom model is expressed as constraint (5) using the SAR definition, where σ and ρ refer to the electric conductivity and the density of the human phantom model, respectively. In this optimization problem, the optimal phase of the transmitted signal can be easily obtained; the condition that $P_R(\mathbf{S})$ is maximum is met when all the polynomial terms of $V_R(\mathbf{S})$ are positive and real. Therefore, the optimal phases of the transmitted signal must be of opposite sign to the phase of the transfer function, that is

$$\psi_n^* = -\phi_n. \tag{6}$$

In terms of the optimal amplitude of the transmitted signal, the optimization problem in (3)–(5) is not a convex problem and belongs to the class of the NP-hard problems. Fortunately, the problem can be transformed to a convex problem.

B. Transformation to Convex Optimization Problem

Equations (3)–(5) can be transformed to an equivalent problem by introducing an auxiliary variable t

$$\min \ 1/t \tag{7}$$

$$\text{s.t.} \ \frac{\|\mathbf{S}\|_F^2}{R} \le P \tag{8}$$

$$t/P_R(\mathbf{S}) \le 1 \tag{9}$$

$$\frac{\sigma\,|\mathbf{E}(r,\mathbf{S})|_F^2}{\rho} \le \text{SAR}, \quad r \in \Psi. \tag{10}$$

This optimization problem is not a geometric program (GP) because the left sides of (9) and (10) are not posynomials. The reason is that the denominator of the left side of (9) is a posynomial and the left side of (10) consists of negative and positive terms. To make this optimization problem a convex problem, the left sides of (9) and (10) need to be transformed to a posynomial. The idea is to use the upper bound of $t/P_R(\mathbf{S})$ as a monomial function [18]. $P_R(\mathbf{S})$ can be expressed as a posynomial function using the optimal phases of the transmitted signal, ψ_n^*. Let $\{f_k(\mathbf{S})\}$ be the monomial terms in posynomial $P_R(\mathbf{S}) = |V_R(\mathbf{S})|^2 = \sum_{k=0}^{K-1} f_k(\mathbf{S})$. K is $N(N+1)/2$. The upper bound can be obtained using the fact that the arithmetic mean is larger than or equal to the geometric mean. Therefore, $\sum_{k=0}^{K-1} f_k(\mathbf{S}) \ge \prod_{k=0}^{K-1} ((f_k\mathbf{S})/x_k)^{x_k}$ with $x_k \ge 0$ and $\sum_{k=0}^{K-1} x_k = 1$, such that the upper bound to the left side of (9) can be approximated by a monomial, that is

$$t/P_R(\mathbf{S}) \le t\prod_{k=0}^{K-1}\left(\frac{f_k(\mathbf{S})}{x_k}\right)^{-x_k}. \tag{11}$$

If the original constraint (9) is tightened by (11), (9) can be replaced by

$$t\prod_{k}\left(\frac{f_k(\mathbf{S})}{x_k}\right)^{-x_k} \le 1. \tag{12}$$

Fortunately, a set of $\{x_k\}$ that tightens the original constraint can be found via an iterative computation method [19], [20]. This method will be explained in detail in the last part of this section. As a result, the left side of (9) is transformed to a monomial, i.e., a posynomial.

In this next step, the left side of (10) is transformed to a posynomial. As $\mathbf{E}(r,\mathbf{S})$ consists of the x, y, and z components of the E-field, we obtain

$$\begin{aligned} &|\mathbf{E}(r,\mathbf{S})|_F^2 \\ &= \sum_{n=0}^{N-1} |e_{xn}(r)|^2 \upsilon_n^2 \\ &\quad + \sum_{n=0}^{N-1} |e_{yn}(r)|^2 \upsilon_n^2 + \sum_{n=0}^{N-1} |e_{zn}(r)|^2 \upsilon_n^2 \\ &\quad + 2\sum_{i=0}^{N-1}\sum_{j=0,i\ne j}^{N-1}\Big[e_{xi}(r)s_i e_{xj}(r)^* s_j^* + e_{yi}(r)s_i e_{yj}(r)^* s_j^* \\ &\qquad + e_{zi}(r)s_i e_{zj}(r)^* s_j^*\Big]. \end{aligned} \tag{13}$$

The first three terms of the right side of (13) are posynomials, whereas all the components of the last term are not. $|\mathbf{E}(r,\mathbf{S})|_F^2$ is a real value; hence, the right side must be a real value. Therefore, (13) can be

replaced by

$$|\mathbf{E}(r,\mathbf{S})|_F^2 = \sum_{n=0}^{N-1} |e_{xn}(r)|^2 v_n^2 + \sum_{n=0}^{N-1} |e_{yn}(r)|^2 v_n^2 + \sum_{n=0}^{N-1} |e_{zn}(r)|^2 v_n^2 + 2\sum_{i=0}^{N-1}\sum_{j=0,i\neq j}^{N-1} |e_{xi}(r)|\,|e_{xj}(r)|\, v_i v_j \cos\theta_l + 2\sum_{i=0}^{N-1}\sum_{j=0,i\neq j}^{N-1} |e_{yi}(r)|\,|e_{yj}(r)|\, v_i v_j \cos\theta_l + 2\sum_{i=0}^{N-1}\sum_{j=0,i\neq j}^{N-1} |e_{zi}(r)|\,|e_{zj}(r)|\, v_i v_j \cos\theta_l \quad (14)$$

where $\theta_l = \psi_i - \psi_j + \phi_i - \phi_j$ for i and j ranging from 0 to $N-1$, $i > j$, and $i \neq j$. Equation (14) can be expressed as $|E(r,\mathbf{S})|^2 = P(r,\mathbf{S}) - N(r,\mathbf{S})$, where $P(r,\mathbf{S})$ and $N(r,\mathbf{S})$ are the sums of the positive terms and negative terms, respectively. Therefore, the inequality in (10) is transformed to $(\sigma P(r,\mathbf{S}))/(\rho SAR + \sigma N(r,\mathbf{S})) \leq 1$ and the same technique used to transform (9) into (11) can be applied. Let $\{f_e(\mathbf{S})\}$ be the monomial terms in a posynomial $\rho SAR + \sigma N(r,\mathbf{S}) = \sum_{e=0}^{E-1} f_e(r,\mathbf{S})$. Therefore, the following inequality holds:

$$\rho SAR + \sigma N(r,\mathbf{S}) \geq \prod_{e=0}^{E-1} \left(\frac{f_e(r,\mathbf{S})}{x_e}\right)^{x_e} \quad (15)$$

where $x_e \geq 0$ and $\sum_{e=0}^{E-1} x_e = 1$. E is the number of positive terms of $\rho SAR + \sigma N(r,\mathbf{S})$ that is not constant with position r.

Finally, the transformed optimization problem can be expressed as

$$\min\ 1/t \quad (16)$$

$$\text{s.t. } \frac{\|\mathbf{S}\|_F^2}{R} \leq P \quad (17)$$

$$t\prod_{k=0}^{K-1}\left(\frac{f_k(\mathbf{S})}{x_k}\right)^{-x_k} \leq 1 \quad (18)$$

$$\sigma P(r,\mathbf{S})\prod_{e=0}^{E-1}\left(\frac{f_e(r,\mathbf{S})}{x_e}\right)^{-x_e} \leq 1, \quad r \in \Psi. \quad (19)$$

The transformed optimization problem expressed by (16)–(19) is the standard GP and a convex problem [18]. The precondition for this optimization problem is that the set of $\{x_k\}$ and $\{x_e\}$ satisfy the tight bounds of (11) and (15). An iterative computation method can be used to find the set of $\{x_k\}$ and $\{x_e\}$ using the approach in [15] and [16] in which the standard GP (16)–(19) is solved for an updated set of $\{x_k\}$ and $\{x_e\}$ at each iteration. To compute $\{x_k\}$ and $\{x_e\}$, the following equations are used:

$$x_k^{(i+1)} = f_k(\mathbf{S}^{(i)}) / \left|V_R(\mathbf{S}^{(i)})\right|^2 \quad (20)$$

$$x_e^{(i+1)} = f_e(r,\mathbf{S}^{(i)}) / \left[\rho \mathrm{SAR} + \sigma N(r,\mathbf{S}^{(i)})\right]. \quad (21)$$

These satisfy the conditions that $x_k \geq 0$, $\sum_{k=0}^{K-1} x_k = 1$, $x_e \geq 0$, and $\sum_{e=0}^{E-1} x_e = 1$ at iteration i. Start with any feasible set $\mathbf{S}$ and compute $\{x_k\}$ and $\{x_e\}$ using (20) and (21). Assuming the solved set of $\mathbf{S}^{(i)}$ at iteration i, compute $x_k^{(i+1)}$ and $x_e^{(i+1)}$ at iteration $i+1$, and solve problem (16)–(19) to obtain $\mathbf{S}^{(i+1)}$. Repeat the iterative computation until convergence. The tight bound conditions of (11) and (15) and the global optimal solution for our MPT system can be found through this iterative method. A summary of the transformation of the original problem (3)–(5) into the convex optimization problem (16)–(19) is shown in Fig. 2.

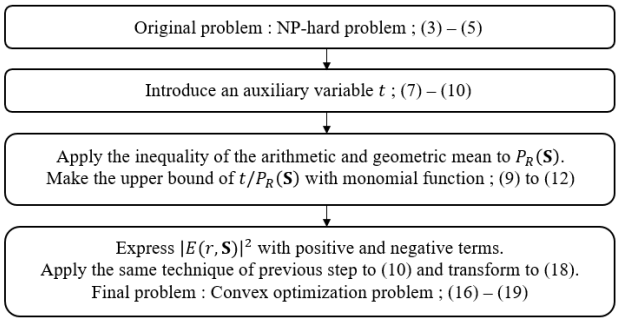

Fig. 2. Flowchart of transformation of the original problem into a convex optimization problem.

III. MPT Simulation Scenario

The 3-D WPT scenario considered for simulation is shown in Fig. 1; the transmitting antenna is a circular array with a radius of 1.5 m comprising 16 bowtie half-lambda dipoles with an operating frequency of 0.9 GHz each. The width, length, thickness, and edge-cutting angle of the bowtie antenna are 55 mm, 143 mm, 0.018 mm, and 55°, respectively. The receiver consists of a single antenna identical to the transmitter and is located at the center of the transmitting array. The phantom is located at a distance d away from the center of the receiver. The dimensions of the phantom are 0.18 m × 0.233 m × 0.96 m, and its dielectric constant, conductivity, and density are 42, 1 S/m, and 1 g/m^3, respectively, as specified in IEC 62232 [21]. The transmitter and receiver are located on the same plane, namely $z = 0$ (center of the phantom). This study considered only the periodic circular array. However, the proposed optimization algorithm can also be used for aperiodic 2-D arrays, such as the one shown in [22].

A full-wave numerical simulation is performed at 0.9 GHz using CST Microwave Studio to obtain E-field data inside the box-shaped phantom for each transmitting antenna. The optimal phases of the transmitted signals can be found using the channel response between the receiver and each transmitting antenna. With the E-field data and the channel responses, the optimal amplitudes of the transmitted signals can be obtained via a MATLAB program using a convex optimization solver, such as CVX [23]. The points for the SAR constraints in the optimization are located 8 mm apart as specified in the IEEE SAR measurement report [24]. They are selected to be 1 mm inside the skin of the phantom because the E-field amplitude is rapidly attenuated with the depth of penetration in the phantom.

The simulation steps are as follows. The optimization region in the phantom consists of several planes. First, the plane, $z = 0$, is chosen because the closest point on the phantom from the receiver is at $z = 0$; then, the optimization algorithm is applied to the phantom plane using the E-field obtained on the selected plane. Then, full-wave numerical simulation is performed using the optimized solution to check if there are any other planes that contain maximum SAR points exceeding 1.6 W/kg averaged over 1 g of the local tissue. If any other plane is detected to have such a point exceeding the SAR constraint, optimization is performed by including that plane. Then, full-wave numerical simulations are used to assess the validity of the solution. These steps are repeated until the maximum SAR is less than or equal to 1.6 W/kg in the entire phantom. The final results, which are the SAR of the box-shaped phantom and the received power satisfying the SAR regulation on the entire phantom, are obtained. In addition, full-wave numerical simulations are performed using the TR technique. A pilot signal transmitted from the receiver is measured at each transmitting antenna. Then, the transmitter excites

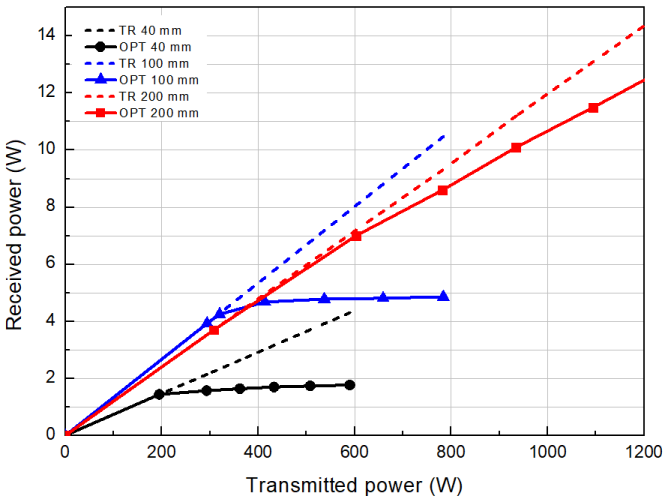

Fig. 3. Comparison of the received power on the receiver using the optimization and TR techniques at 0.9 GHz with 16 transmitting antennas. The solid lines represent the optimization technique. The dashed lines represent the calculated results of the TR technique, which cannot be obtained considering SAR constraints. The black, blue, and red lines indicate the distances of 40, 100, and 200 mm, respectively. The symbols indicate the simulated points.

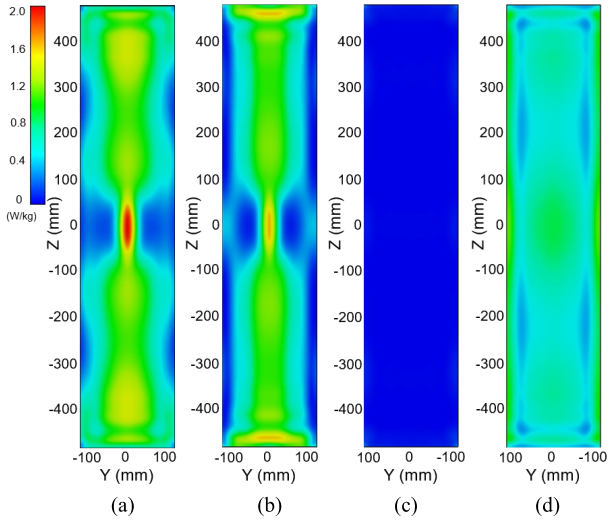

Fig. 4. Magnitude of the SAR distribution in the front and rear of the box-shaped phantom relative to the receiver when the received power is 1.76 W, which is the maximum received power for the OPT technique in the worst case MPT scenario. (a) Front and (c) rear distributions using the TR technique. (b) Front and (d) rear distributions using the proposed optimization technique.

the phase-conjugated signal of the measured signal to obtain the results of the TR technique.

The MPT scenarios are simulated with various distances between the phantom and the receiver. We simulate MPT scenarios in which the distance varied from 40 to 200 mm. The phantom is located closest to the receiver when $d = 40$ mm, which is the worst case scenario according to the SAR test report published by the FCC [25]. In addition, scenarios with either 8 or 16 transmitting antennas are simulated.

IV. Results and Discussion

The results of the proposed optimization technique are compared with those of the TR technique as a reference for MPT. In the time-harmonic case, the TR technique transmits the phase-conjugated signal of the pilot signal generated from the receiver at each transmitting antenna [7]. The received power relative to the transmitted power for each distance d between the phantom and receiver is shown in Fig. 3.

A. Worst Case Analysis

In this section, the worst case of the MPT scenario is explained in detail. The received power of the OPT technique is the same as that of the TR technique up to a transmitted power of 195 W, as shown in the black solid line in Fig. 3. TR is the optimal solution of the OPT technique until the maximum SAR of the phantom exceeds the limit with the maximum PTE [7]. The received power and the maximum SAR of the TR technique increase proportionally with the transmitted power. It is due to the fact that the PTE of the TR technique and the proportion of the transmitted power at each transmitting antenna are constant even if the transmitted power changes. Therefore, for a transmitted power higher than 195 W with TR technique, the maximum SAR exceeds the limit of 1.6 W/kg. If the SAR constraint is not considered, the TR technique can transfer more power, as shown by the black dashed line in Fig. 3. On the other hand, the OPT technique, which uses the optimal input signal obtained via the optimization algorithm, makes the peak E-field in the phantom lower even for a transmitted power higher than 195 W. As a result, the maximum SAR is maintained at 1.6 W/kg and the received power saturates to 1.76 W as the transmitted power increases. Therefore, the OPT technique transfers more power than the TR technique and the results show that the proposed optimization algorithm can be used in the worst case MPT scenario.

The SAR distribution of the box-shaped phantom is shown in Fig. 4 for the worst case WPT scenario with a transmitted power of 600 W to elucidate the operation of the OPT technique. The magnetic field distribution is not shown here because the phantom is located in the far-field region of the transmitting antenna even though it should be considered to be in the near-field region [26]. The input reflection coefficient of the receiver is increased in the worst case scenario due to the near-phantom effect compared with other scenarios. However, it does not affect the comparison result between TR and OPT because its effect is included equally in both these cases. When the TR technique is used, the maximum SAR is 2 W/kg at the phantom in front of the receiver, which exceeds the SAR limit (1.6 W/kg), as shown in Fig. 4(a). However, with the OPT technique, the maximum SAR is 1.6 W/kg, and the SAR is relatively uniformly distributed on the phantom and is below 1.6 W/kg, as shown in Fig. 4(b) and (d).

It is worth noting that the SAR distributions on the rear of the phantom using the TR and OPT techniques are clearly different, as shown in Fig. 4(c) and (d). The SAR obtained through the TR technique is approximately zero because the channel responses of the transmitting antennas at the rear of the phantom and receiver are significantly lower than those of the other antennas. However, the SAR obtained through the OPT technique has a higher but limited value. According to the ANSI/IEEE C95.1 standard, only the peak SAR is relevant when assessing human safety [13]. Therefore, in the OPT technique, the value of the SAR need not be zero anywhere in the phantom, and the transmitters behind the phantom transmit more power than those in the TR technique even though the channel responses between the receiver and transmitters are lower. This is because the target of the optimization problem is to maximize received power and not the PTE. Therefore, the PTE of the OPT technique is equal to or lower than that obtained via the TR technique. Because of this difference between the TR and OPT techniques, the maximum SAR of the TR technique exceeds 1.6 W/kg, whereas the OPT technique satisfies the SAR regulation when both receive same power.

TABLE I

PERFORMANCE COMPARISON OF TR AND OPT TECHNIQUES WITH 16 TRANSMITTING ANTENNAS SATISFYING THE SAR CONSTRAINT

Distance between receiver and phantom	Time-Reversal		Optimization	
	Maximum Received Power (W)	PTE (%)	Maximum Received Power (W)	PTE (%)
40 mm	1.43	0.73	1.76	0.29
100 mm	3.93	1.34	4.86	0.62
200 mm	3.70	1.22	15.6	0.87

TABLE II

EXCITATION OF 16 TRANSMITTING ANTENNAS AT THE POINT OF MAXIMUM RECEIVED POWER SATISFYING THE SAR CONSTRAINT

Distance / Transmitter number	40 mm		100 mm		200 mm	
	TR (V)	OPT (V)	TR (V)	OPT (V)	TR (V)	OPT (V)
1	8.77	8.08	8.40	2.65	5.42	4.69
2 (16)	8.22	7.43	8.40	6.43	4.90	1.31
3 (15)	7.12	7.11	8.64	10.40	5.16	12.11
4 (14)	4.93	4.20	7.44	9.69	8.00	31.91
5 (13)	3.29	7.22	5.76	5.20	9.30	12.00
6 (12)	1.92	7.32	3.60	8.16	7.74	10.61
7 (11)	0.82	3.34	3.34	12.55	4.64	16.71
8 (10)	0.27	17.02	1.90	0	1.29	2.73
9	0.82	6.14	0.22	23.77	1.14	12.31

B. Effect of Separation Between Receiver and Phantom

The performance of the OPT and TR techniques with respect to the distance between the receiver and the phantom is shown in Fig. 3. In addition, the maximum received power and the PTE while satisfying the SAR constraint are reported in Table I. The maximum received power of both techniques is increased by increasing the distance between the receiver and the phantom. When the TR technique is used, the maximum received power for a distance of 200 mm is 157% higher than in the 40 mm case. If the separation is larger, the EMF loss on the phantom decreases because the transmitter focuses EMF on the receiver. In addition, the PTE of the TR technique increases by 67% because the number of non-line-of-sight (NLOS) paths between the transmitting antennas and the receiver decreases from 7 to 3. The magnitude of the channel response of the line of sight (LOS) paths is larger than that of the NLOS paths by a factor of 3 or more, as listed in Table II. Therefore, the PTE of the TR technique is higher when the separation is larger because the number of NLOS paths decreases.

In the OPT technique, the maximum received power increases by 781% for a distance of 200 mm compared with the 40 mm case, which is higher than that of the TR technique by a factor of 5. The OPT algorithm prioritizes LOS paths to transfer more power to the receiver because of the larger magnitude of the channel response than on the NLOS paths. Therefore, the transmitting antennas assign as much power as possible to the LOS paths in such a way that the maximum SAR of the phantom does not exceed the SAR limit. Next, the OPT algorithm excites the transmitting antennas having NLOS paths without increasing the peak SAR because almost all the EMF is absorbed in the rear of the phantom. Therefore, having many LOS paths is advantageous in order to increase the maximum received power and PTE. In other words, the number of LOS paths is the degree of freedom of the optimization algorithm.

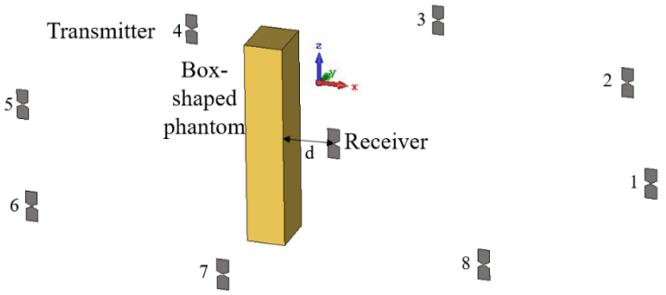

Fig. 5. 3-D MPT scenario with eight transmitters and a receiver comprising bowtie half-lambda dipole antennas and small a box-shaped phantom near the receiver.

The excitation of each transmitting antenna when the maximum power is transferred for each distance is presented in Table II. To analyze how the transmitted power is wasted when using the OPT technique compared with the TR technique, the figure of merit (FOM) is defined as the OPT to TR ratio in terms of the transmitted power on each path. If more power than the proportion of the channel response in the TR technique is assigned to an NLOS path, the PTE of the entire MPT system decreases. For a distance of 40 mm, the paths between the transmitters 6 through 9 and the receiver are NLOS paths and, hence, the amplitudes of the channel responses are lower than on the other paths, as shown in the TR results. The FOMs of the NLOS paths are larger than 14, whereas those of the other paths are lower than 5. Therefore, the PTE of the OPT technique is much lower than that of the TR technique. The paths between the transmitters 8 and 9 and the receiver are NLOS paths for distances of 100 and 200 mm. FOM of path 9 is only dominantly larger than those of other paths in both cases. Therefore, the rate at which the PTE decreases when using the OPT technique compared with the TR technique at distances of 100 and 200 mm is less than that at a distance of 40 mm.

The maximum received power with the OPT technique is 23% higher than with the TR technique, although the PTE is 60% lower for a distance of 40 mm, as presented in Table I. The PTE of the OPT technique decreases because of several NLOS paths. However, the rate at which the maximum received power increases compared with the TR technique becomes higher as the distance increases. For a distance of 200 mm, the maximum received power is 322% higher and the PTE is 29% lower with OPT technique than the TR technique. Note that the OPT technique outperforms the TR technique in every scenario, particularly when the distance is 200 mm. In addition, it is found that the results with an SAR limit of 2 W/kg averaged over 10 g of local tissue show that more power can be received with the OPT technique than the TR technique. The PTE in this study is quite low because the antennas used have omnidirectional patterns and the number of transmitting antennas is inadequate to focus the EMF.

C. Effect of the Number of Transmitting Antennas

The scenario with a lower number of transmitting antennas, i.e., eight, is considered, as shown in Fig. 5. The performances of the TR and OPT techniques are presented in Table III. The PTE of the TR technique decreases by more than 50% compared with the

TABLE III

PERFORMANCE COMPARISON OF TR AND OPT TECHNIQUES WITH EIGHT TRANSMITTING ANTENNAS SATISFYING THE SAR CONSTRAINT

Distance between receiver and phantom	Time-Reversal		Optimization	
	Maximum Received Power (W)	PTE (%)	Maximum Received Power (W)	PTE (%)
40 mm	1.43	0.28	1.56	0.18
100 mm	3.85	0.54	4.6	0.41
200 mm	3.35	0.49	5.76	0.38

scenario with 16 transmitting antennas because the electric area of the transmitter is reduced by 50% [9]. When the number of transmitting antennas decreases at a distance of 200 mm, it is noted that the increasing rate of the LOS path number to the total path number is lower compared with other scenario, which explains larger decreasing rate of PTE of the OPT technique. The maximum received power of the OPT and TR techniques is slightly lower compared with the corresponding cases with 16 transmitting antennas. These results demonstrate that the OPT technique can be used even with a small number of transmitting antennas. In all cases, the maximum received power obtained using the OPT technique is higher than that obtained using the TR technique, even though the PTE of the OPT technique is lower.

V. CONCLUSION

In this communication, we have proposed the new convex optimization algorithm for the design of an MPT system that transfers the maximum allowable power while satisfying an SAR constraint for human safety. The optimization problem for our MPT scenario is formulated and transformed into an equivalent convex optimization problem using various techniques, and the optimal amplitudes and phases of the transmitting antenna array are obtained. The results are then compared with those obtained using the TR technique, which is known as the optimal solution in MPT. The optimization technique can receive higher power with a lower PTE compared with the TR technique in the worst case scenario, which is clearly explained with the SAR distributions in the phantom and excitation signals. The received power and PTE are calculated for various distances between the receiver and phantom and for different number of transmitting antennas. The results indicate that the OPT technique transfers more power to the receiver than the TR technique in the MPT scenarios considered, particularly in the case where the distance between the receiver and the phantom is larger. In addition, the maximum received power obtained using the OPT technique is higher than that obtained using the TR technique even for a lower number of transmitting antennas. Therefore, the OPT technique outperforms the TR technique in terms of faster charging via MPT for every scenario considered. The results of this communication, which considered practical MPT scenarios, are expected to be useful for implementing the proposed optimization algorithm during the design of MPT systems with SAR constraints to ensure human safety.

REFERENCES

[1] B. Strassner and K. Chang, "Microwave power transmission: Historical milestones and system components," *Proc. IEEE*, vol. 101, no. 6, pp. 1379–1396, Jun. 2013.

[2] A. Costanzo and D. Masotti, "Smart solutions in smart spaces: Getting the most from far-field wireless power transfer," *IEEE Microw. Mag.*, vol. 17, no. 5, pp. 30–45, May 2016, doi: 10.1109/MMM.2016.2525119.

[3] W. Brown, "Experiments involving a microwave beam to power and position a helicopter," *IEEE Trans. Aerosp. Electron. Syst.*, vol. AES-5, no. 5, pp. 692–702, Sep. 1969.

[4] P. E. Glaser, "Power from the sun: Its future," *Science*, vol. 162, no. 3856, pp. 857–861, Nov. 1968.

[5] Y. Li and V. Jandhyala, "Design of retrodirective antenna arrays for short-range wireless power transmission," *IEEE Trans. Antennas Propag.*, vol. 60, no. 1, pp. 206–211, Jan. 2012.

[6] M. Ettorre, W. A. Alomar, and A. Grbic, "2-D Van Atta array of wideband, wideangle slots for radiative wireless power transfer systems," *IEEE Trans. Antennas Propag.*, vol. 66, no. 9, pp. 4577–4585, Sep. 2018.

[7] W. Geyi, *Foundations of Applied Electrodynamics*. New York, NY, USA: Wiley, 2010.

[8] J. de Rosny, G. Lerosey, and M. Fink, "Theory of electromagnetic time-reversal mirrors," *IEEE Trans. Antennas Propag.*, vol. 58, no. 10, pp. 3139–3149, Oct. 2010.

[9] J.-H. Kim, Y. Lim, and S. Nam, "Efficiency bound of radiative wireless power transmission using practical antennas," *IEEE Trans. Antennas Propag.*, vol. 67, no. 8, pp. 5750–5755, Aug. 2019.

[10] R. Ibrahim *et al.*, "Experiments of time-reversed pulse waves for wireless power transmission in an indoor environment," *IEEE Trans. Microw. Theory Techn.*, vol. 64, no. 7, pp. 2159–2170, Jul. 2016.

[11] A. Boaventura, D. Belo, R. Fernandes, A. Collado, A. Georgiadis, and N. B. Carvalho, "Boosting the efficiency: Unconventional waveform design for efficient wireless power transfer," *IEEE Microw. Mag.*, vol. 16, no. 3, pp. 87–96, Apr. 2015.

[12] B. Clerckx and E. Bayguzina, "Waveform design for wireless power transfer," *IEEE Trans. Signal Process.*, vol. 64, no. 23, pp. 6313–6328, Dec. 2016.

[13] *IEEE Standard for Safety Levels With Respect to Human Exposure to Radio Frequency Electromagnetic Fields, 3 kHz to 300 GHz*, IEEE Standard C95.1-2005, Apr. 2006.

[14] C. Liu, Y.-X. Guo, H. Sun, and S. Xiao, "Design and safety considerations of an implantable rectenna for far-field wireless power transfer," *IEEE Trans. Antennas Propag.*, vol. 62, no. 11, pp. 5798–5806, Nov. 2014.

[15] G. Kim, S. Boo, S. Kim, and B. Lee, "Control of power distribution for multiple receivers in SIMO wireless power transfer system," *J. Electromagn. Eng. Sci.*, vol. 18, no. 4, pp. 221–230, Oct. 2018.

[16] M. Koohestani, M. Zhadobov, and M. Ettorre, "Design methodology of a printed WPT system for HF-band mid-range applications considering human safety regulations," *IEEE Trans. Microw. Theory Techn.*, vol. 65, no. 1, pp. 270–279, Jan. 2017.

[17] D. A. M. Iero, T. Isernia, and L. Crocco, "Focusing time-harmonic scalar fields in complex scenarios: A comparison," *IEEE Antennas Wireless Propag. Lett.*, vol. 12, pp. 1029–1032, 2013.

[18] R. J. Duffin and E. L. Peterson, "Geometric programming with signomials," *J. Optim. Theory Appl.*, vol. 11, no. 1, pp. 3–35, Jan. 1973.

[19] M. Chiang, *Geometric Programming for Communication Systems* (Foundations and Trends in Communications and Information Theory). Delft, The Netherlands: Now, 2005.

[20] C. S. Beightler and D. T. Phillips, *Applied Geometric Programming*. Hoboken, NJ, USA: Wiley, 1976.

[21] *Determination of RF Field Strength and SAR in the Vicinity of Radiocommunication Base Stations for the Purpose of Evaluating Human Exposure*, document IEC 62232, May 2011.

[22] A. F. Morabito, "Power synthesis of mask-constrained shaped beams through maximally-sparse planar arrays," *Telecommun. Comput. Electron. Control*, vol. 14, no. 4, pp. 1217–1219, 2016.

[23] M. Grant, S. Boyd, and Y. Ye. (2015). *CVX: MATLAB Software for Disciplined Convex Programming*. [Online]. Available: http://cvxr.com/cvx/

[24] *IEEE Recommended Practice for Determining the Peak Spatial-Average Specific Absorption Rate (SAR) in the Human Head From Wireless Communications Devices: Measurement Techniques*, IEEE Standard 1528-2013 (Revision IEEE Std 1528-2003), Sep. 2013, pp. 1–246, doi: 10.1109/IEEESTD.2013.6589093.

[25] UL Verification Services INC, Energous Corporation, San Jose, CA, USA. (2017). *SAR Evaluation Report*. Accessed: Sep. 19, 2017. [Online]. Available: https://fccid.io/2ADNG-MS300/RF-Exposure-Info/SAR-report-V3-368490

[26] N. Kuster and Q. Balzano, "Energy absorption mechanism by biological bodies in the near field of dipole antennas above 300 MHz," *IEEE Trans. Veh. Technol.*, vol. 41, no. 1, pp. 17–23, 1st Quart., 1992.